A Scalable Cryo-CMOS 2-to-20GHz Digitally Intensive Controller for 4×32 Frequency Multiplexed Spin Qubits/Transmons in 22nm FinFET Technology for Quantum Computers

Patra, Bishnu; Van Dijk, Jeroen P.G.; Corna, Andrea; Xue, Xiao; Samkharadze, Nodar; Sammak, Amir; Scappucci, Giordano; Veldhorst, Menno; Vandersypen, Lieven M.K.; Babaie, Masoud

**Citation (APA)**
Patra, B., Van Dijk, J. P. G., Corna, A., Xue, X., Samkharadze, N., Sammak, A., Scappucci, G., Veldhorst, M., Vandersypen, L. M. K., Babaie, M., Sebastiano, F., Charbon, E., & More Authors (2020). A Scalable Cryo-CMOS 2-to-20GHz Digitally Intensive Controller for 4×32 Frequency Multiplexed Spin Qubits/Transmons in 22nm FinFET Technology for Quantum Computers. In *2020 IEEE International Solid-State Circuits Conference, ISSCC 2020* (Vol. 2020-February, pp. 304-306). Article 9063109 IEEE. https://doi.org/10.1109/ISSCC19947.2020.9063109

**Important note**
To cite this publication, please use the final published version (if applicable).
Please check the document version above.

**A Scalable Cryo-CMOS 2-to-20GHz Digitally-Intensive Controller for $4\times32$ Frequency Multiplexed Spin Qubits/Transmons in 22-nm FinFET Technology for Quantum Computers**

Quantum computers (QC), comprising qubits and a classical controller, can provide exponential speed-up in solving certain problems. Among solid-state qubits, transmons and spin-qubits are the most promising, operating $\ll$1K. A qubit can be implemented in a physical system with two distinct energy levels representing the $|0\rangle$ and $|1\rangle$ states, e.g. the up and down spin states of an electron. The qubit states can be manipulated with microwave pulses, whose frequency $f$ matches the energy level spacing $E = hf$ (Fig. 1). For transmons, $f\sim$6GHz, for spin qubits $f\sim$20GHz, with the desire to lower it in the future. Qubit operations can be represented as rotations in the Bloch sphere. The rotation axis is set by the phase of the microwave signal relative to the qubit phase, which must be tracked for coherent operations. The pulse amplitude and duration determine the rotation angle. A $\pi$-rotation is typically obtained using a 50-ns Gaussian pulse for transmons and a 500-ns rectangular pulse for spin qubits with powers of -60dBm and -45dBm, respectively.

State-of-the-art QCs, with only a few qubits, are typically driven by room temperature (RT) electronics, with a single RF-cable per qubit (Fig. 1). A fault-tolerant QC requires millions of qubits [1], making RT control impractical due to interconnect complexity. To address this, a fully-integrated cryogenic control system close to the qubits has been proposed [2]. A cryogenic pulse modulator has been demonstrated [3], however its scalability is limited by the need of one LO and cable per qubit, and external circuitry for LO leakage cancellation, as the LO is at the qubit frequency. Moreover, the used fixed-length symmetric pulses limit theoretically achievable operation fidelity and compatible qubit technologies. In this work, we present a scalable controller that (a) exploits FDMA to reduce the number of RF-cables per qubit (Fig. 1), (b) features arbitrary I/Q pulse generation for high-fidelity operation over a wide frequency (>4$\times$ higher than [3]) and output power range to support both spin qubits and transmons, and (c) can be directly integrated in an existing quantum control stack thanks to a digitally-intensive architecture with integrated instruction set.

A controller employing FDMA requires both a wide bandwidth to accommodate many qubits, each with a unique frequency [4], and pulse shaping to minimize spectral leakage to other qubits. To allow 99.99% fidelity for a $\pi$-

rotation, exceeding the state-of-the-art, an SFDR $>$44dB is required to avoid disturbing unaddressed qubits [5]. This demands a linear transmitter architecture with good image and LO leakage rejection. For this fidelity, 44dB SNR is also required in a 25 MHz noise bandwidth. To control both spin qubits and transmons, we designed for a 2-20GHz output frequency range, 40dB gain control, and flexible I/Q pulse shaping with 1ns to 40μs duration.

Fig. 2 shows the block diagram of the system, comprising an instruction controller, a DDS and an analog/RF front-end. For coherent control of 32 qubits, 32 numerically controlled oscillators (NCO) with 0.2kHz frequency resolution are used, allowing the use of a single external LO. The DDS is clocked at 1GHz considering the number of qubits (N) and a required bandwidth of 30MHz/qubit [5]. A polar modulator is used to efficiently produce the desired pulse for each qubit at such a high clock frequency. The signals of two banks are combined in I/Q domain to achieve SSB up-conversion over a large data bandwidth. To achieve the required SFDR, digital I/Q and offset calibration networks are implemented for image and LO leakage rejection ($\alpha$, $\beta$, $\gamma$ in Fig. 1). As signal replicas of the 10-bit segmented (5T-5B) current-steering DAC (see Fig. 2) can fall in-band after up-conversion to low carrier frequencies, a 2$^{nd}$ order gm-C reconstruction filter is used. High linearity is achieved by utilizing current-bleeding in the DAC and current-mode operation in the filter.

The required gain control is achieved with $>$200 steps, by a baseband VGA, implemented as tunable current mirror, in combination with a tunable-gain RF amplifier. The current mirror feeds the current into a quadrature double-balanced Gilbert-cell active mixer with current-bleeding driven by an on-chip LO driver and active balun. To cover a 2-20GHz output band, the RF path is split into 2 parts with the high band using the 3$^{rd}$ harmonic of the LO for up-conversion. Cascode switches are used at the mixer output to steer the current either into a resistor for the RF-Low band (2-15 GHz) or a transformer tuned to $3f_{LO}$ for the RF-High band (15-20 GHz). The class-A amplifiers with wideband output baluns drive qubits over a 50-$\Omega$ cable.

The chip was fabricated in 22-nm FinFET CMOS with a total area of 16mm$^2$ comprising 4 controllers ($M$), flip-chip bonded to a BGA package (Fig. 7). A custom-made annealed and gold-plated copper enclosure was designed for efficient cooling and mounting of the PCB in a dilution refrigerator.

Fig. 3 shows the measured peak output power at 3K over 2-20GHz, with flatness limited by additional ground

inductance introduced in the layout. The sampling replicas are highly attenuated by the filter, as measured at the BB-out test port. The peak output power SFDR is >45dB, equally limited by HD2 and image rejection ratio (IRR). The LO rejection ratio (LORR) of 36dB after calibration does not limit the SFDR, as this is not a favorable band for qubit control in a direct conversion topology and can be avoided by proper choice of $f_{LO}$. Measured IM3 and SNR (25MHz bandwidth) are better than 50dB and 48dB respectively.

The amplitude and phase modulation information for pulse shaping (18Gb/s) is stored in on-chip SRAM allowing envelopes up to 41μs, which are referenced by a look-up table (LUT) that can define 8 instructions per qubit (Fig. 4), each with a phase offset to efficiently re-use envelopes for different rotation axes. The use of instruction tables reduces the required data rate to the controller, which is further reduced to ~1kb/s by the integrated programmable instruction set executed on external trigger with minimal delay between instructions. The versatility of this design is demonstrated in Fig. 4 showing the measurement of an instruction sequence containing 5 unique waveforms targeting 5 different qubit frequencies.

To demonstrate qubit control, a Rabi-experiment is performed at 14GHz and 18GHz on a sample with one single-electron silicon spin qubit (Fig. 5, top), in which the qubit state is rotated over an increasing angle by a pulse of incrementing duration $t$. For a fair comparison, the chip is left connected to the qubit with only the digital turned on when using the RT setup, to avoid any change in qubit parameters. The performance of the quantum processor when driven by our controller is similar to that of the RT setup (specifications in Fig. 6), limited by the readout fidelity due to the qubit energy level spacing being comparable to the thermal energy. To demonstrate coherent control, rotations around different axes are performed by executing two $\pi/2$-rotations around the X-axis interposed by a Z-rotation with *varying* angle $\theta$ obtaining the expected cosine shape (Fig. 5, bottom). The Z-rotation is implemented using the built-in Z-correction (designed to compensate for Stark-shift due to crosstalk in an FDMA scheme [4]) that can automatically apply an instruction-dependent phase correction (Z-corr., Fig. 1) to any NCO.

Compared to state-of-the-art qubit controller ICs (Fig. 6), this work exhibits a wide frequency and output power range compatible with multiple qubit technologies. The frequency multiplexing architecture potentially enables multi-qubit control over a single RF-cable, leading to a scalable system. The digitally-intensive architecture enables

waveform shaping flexibility, minimum execution latency and straightforward integration in the existing quantum computing stack.

## References

[1] A. G. Fowler et al., "Surface codes: Towards practical large-scale quantum computation," *Physical Review A*, vol. 86, no. 3, p. 032324, 2012.

[2] E. Charbon et al., "Cryo-CMOS circuits and systems for scalable quantum computing," *ISSCC Dig. Tech. Papers*, pp. 264-265, 2017.

[3] J. C. Bardin et al., "A 28nm Bulk-CMOS 4-to-8GHz <2mW Cryogenic Pulse Modulator for Scalable Quantum Computing," *ISSCC Dig. Tech. Papers*, pp. 456-458, 2019.

[4] M. Veldhorst et al., "A two-qubit logic gate in silicon," *Nature 526.7573*, pp. 410, 2015.

[5] J. P. G. van Dijk et al., "The impact of classical control electronics on qubit fidelity," *arXiv preprint arXiv:1803.06176*, 2018.

[6] C. A. Ryan, B. R. Johnson, D. Ristè, B. Donovan and T. A. Ohki, "Hardware for dynamic quantum computing," *Rev. Sci. Instrum.*, 2017.
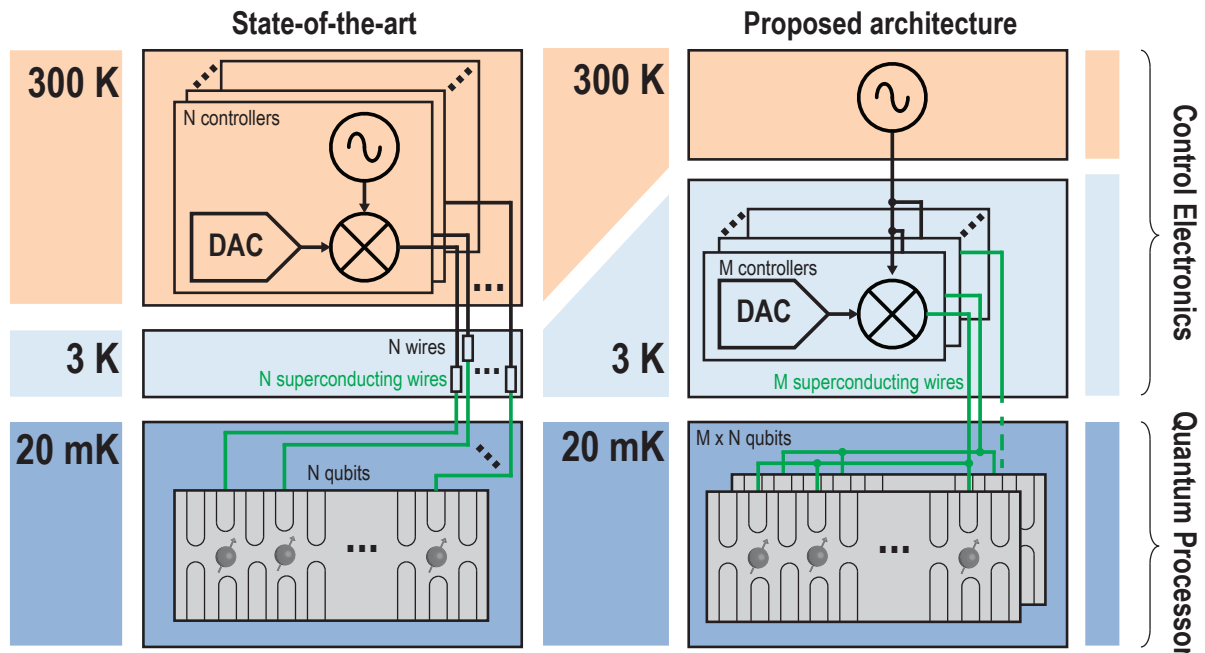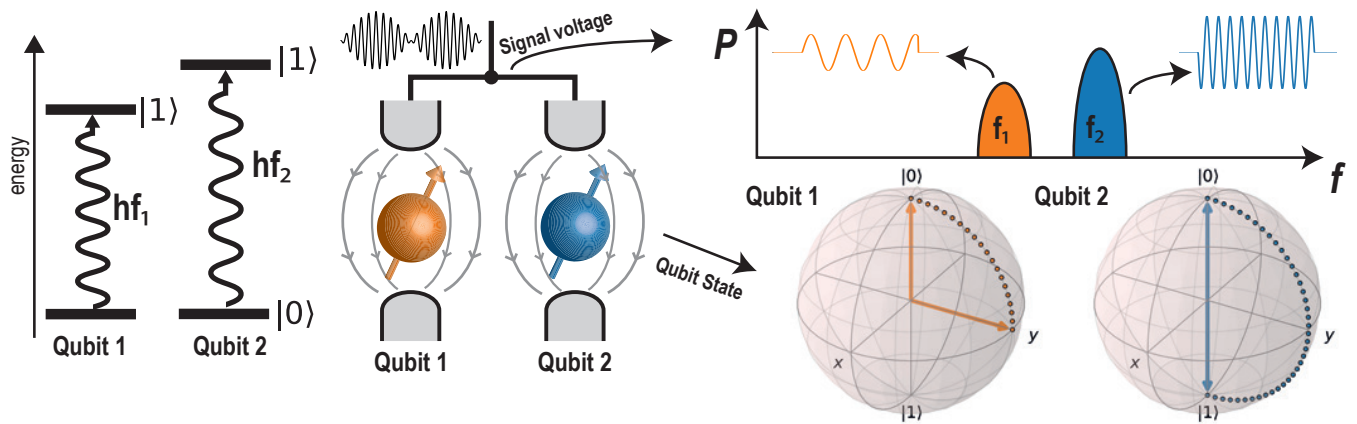
**Fig. 1:** Qubit control signals, current state-of-the-art controller and proposed cryogenic controller with frequency multiplexing.
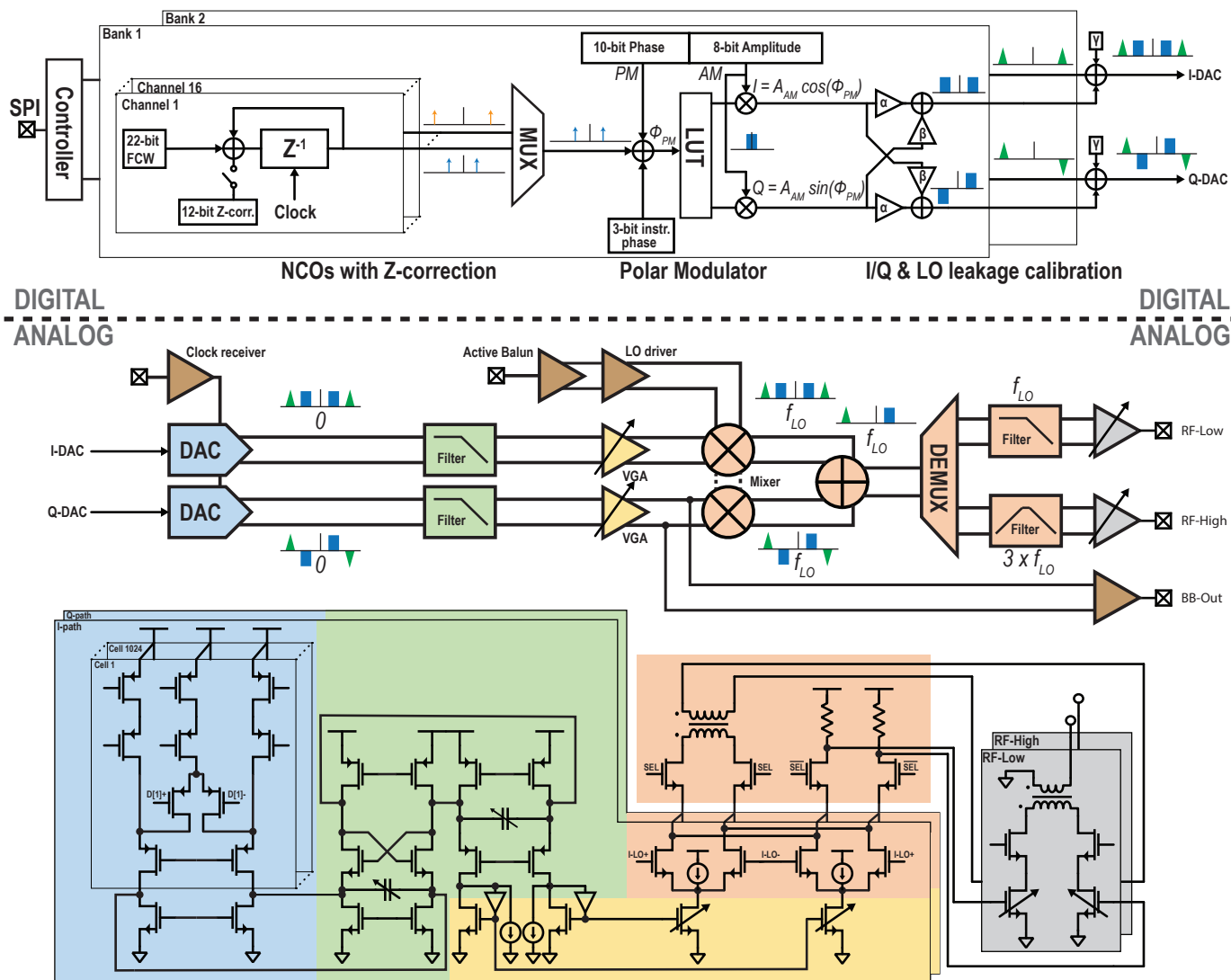
**Fig. 2:** Block diagram and transistor level schematic (bias circuitry not shown).
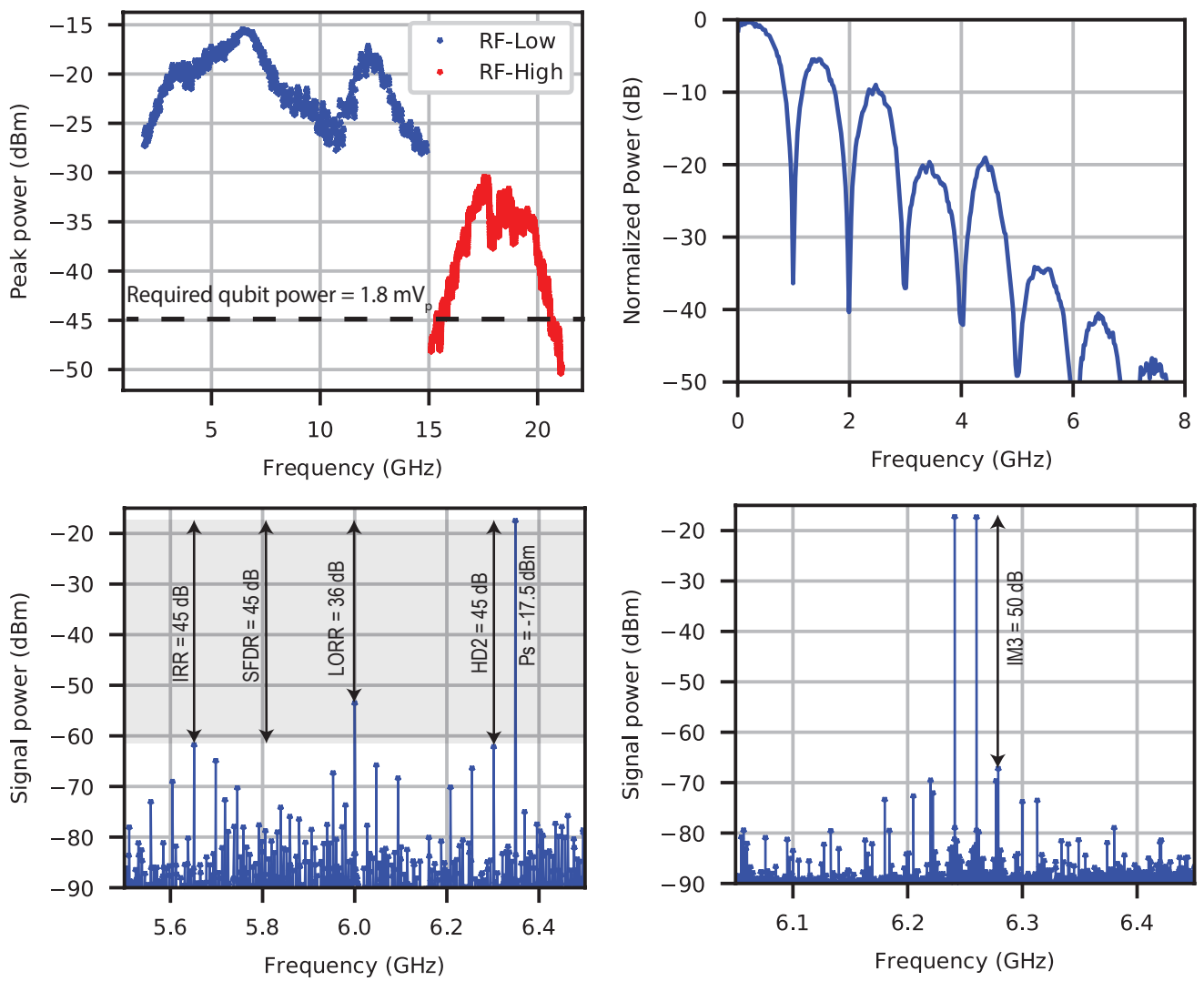
**Fig. 3: Measured RF Bandwidth, BB-Out transfer function, RF-Low output with NCO frequency at 350 MHz, two-tone RF-Low output with NCO frequencies at 241 MHz & 260 MHz, all at 3 K.**
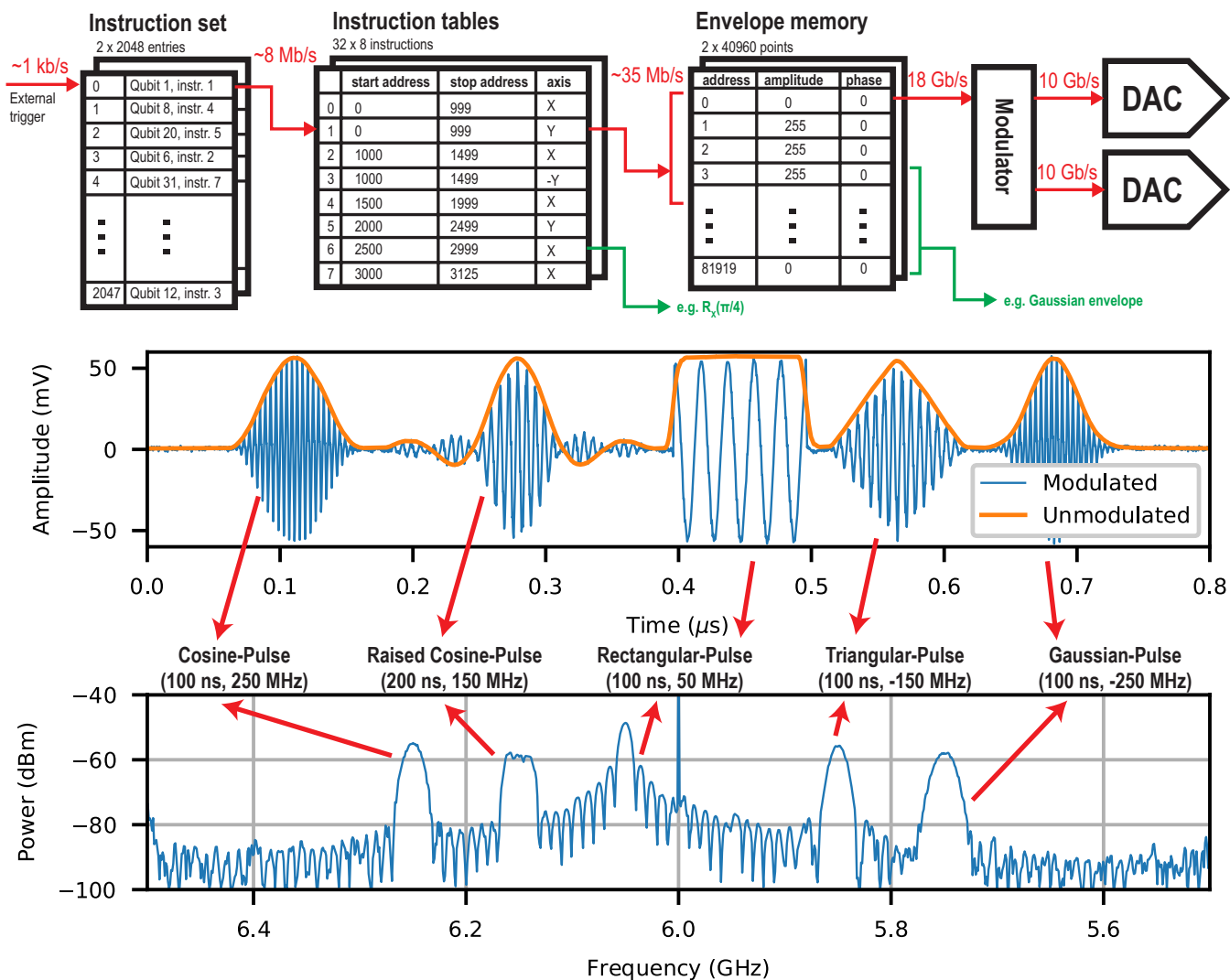
**Instruction set**
2 x 2048 entries

| | |
|---|---|
| 0 | Qubit 1, instr. 1 |
| 1 | Qubit 8, instr. 4 |
| 2 | Qubit 20, instr. 5 |
| 3 | Qubit 6, instr. 2 |
| 4 | Qubit 31, instr. 7 |
| ⋮ | ⋮ |
| 2047 | Qubit 12, instr. 3 |

~1 kb/s
External trigger

~8 Mb/s

**Instruction tables**
32 x 8 instructions

| | start address | stop address | axis |
|---|---|---|---|
| 0 | 0 | 999 | X |
| 1 | 0 | 999 | Y |
| 2 | 1000 | 1499 | X |
| 3 | 1000 | 1499 | -Y |
| 4 | 1500 | 1999 | X |
| 5 | 2000 | 2499 | Y |
| 6 | 2500 | 2999 | X |
| 7 | 3000 | 3125 | X |

~35 Mb/s

**Envelope memory**
2 x 40960 points

| address | amplitude | phase |
|---|---|---|
| 0 | 0 | 0 |
| 1 | 255 | 0 |
| 2 | 255 | 0 |
| 3 | 255 | 0 |
| ⋮ | ⋮ | ⋮ |
| 81919 | 0 | 0 |

18 Gb/s

**Modulator**

10 Gb/s → **DAC**

10 Gb/s → **DAC**

e.g. $R_x(\pi/4)$

e.g. Gaussian envelope

Cosine-Pulse (100 ns, 250 MHz)

Raised Cosine-Pulse (200 ns, 150 MHz)

Rectangular-Pulse (100 ns, 50 MHz)

Triangular-Pulse (100 ns, -150 MHz)

Gaussian-Pulse (100 ns, -250 MHz)

**Fig. 4: Qubit pulse shaping; top-to-bottom: digital backend, measured BB-Out signal and RF-Low spectrum (LO at 6 GHz), both at 3 K.**
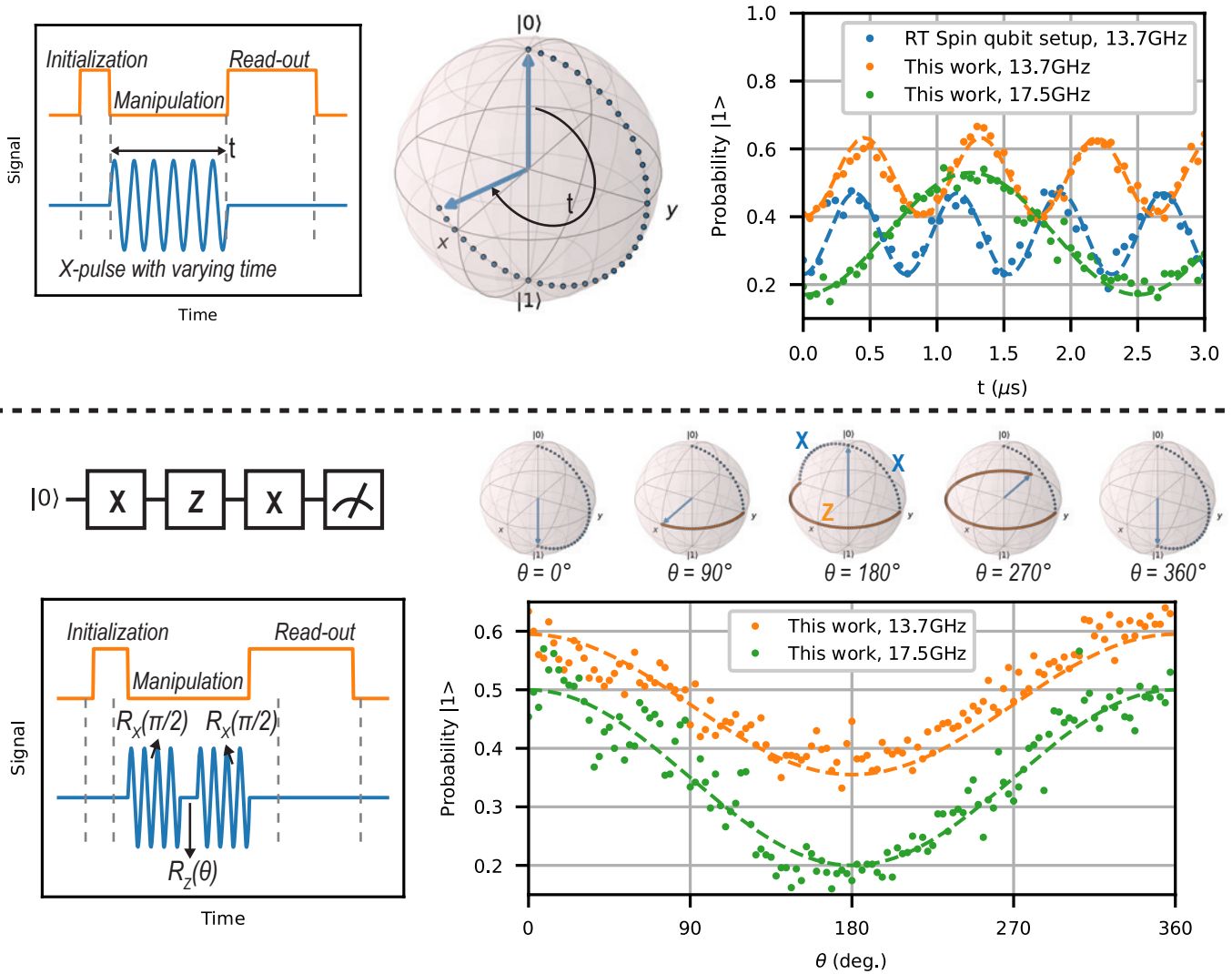
**Fig. 5:** Rabi oscillation and coherent qubit control experiments at 14 GHz and 18 GHz with the controller IC at 3 K.

| | This work | ISSCC'19 [3] | RSI'17 [6] | Spin qubit setup |
|---|---|---|---|---|
| Operating Temperature | 3 K | 3 K | 300 K | 300 K |
| Qubit platform | **Transmons + spin qubits** | Transmons | Transmons | Spin qubits |
| Qubit frequency | **2-20 GHz** | 4-8 GHz | | < 20 GHz |
| Channels | **128 (32 per TX)** | 1 | 4 | 1 |
| FDMA | **Yes, SSB** | No | Yes, SSB | No |
| Sampling rate | 1 GS/s | 1 GS/s | 1.2 GS/s | 1.2 GS/s |
| Data Bandwidth | 1 GHz | 400 MHz | 960 MHz | 520 MHz |
| SFDR$^{\dagger}$ | > 45 dB | N/A | | 70 dB |
| IM3 ($\Delta$f = 19 MHz) | > 50 dB | N/A | | |
| SNR (BW = 25 MHz) | 48 dB | N/A | | |
| Noise Floor >10MHz | < -144 dBm/Hz (At -19 dBm) | N/A | | -138 dBm/Hz (At +10 dBm) |
| Image & LO leakage calibration | **On chip** | Off chip | Yes | |
| Waveform/ Instructions | **upto 40960 points AWG** | Fixed 22 points symmetric | | 16M points AWG |
| Instruction set | **Yes** | No | Yes | Yes |
| Automatic Z-corr. | **Yes** | No | No | No |
| Power / TX | Analog: 1.7 mW/qubit* Digital: 330 mW$^{\ddagger}$ | Analog: <2 mW/qubit$^{\#}$ Digital: N/A | | 850 W |
| Chip area / TX | 4 mm$^2$ | 1.6 mm$^2$ | Discrete components | Rack mount |
| Technology | 22 nm FinFET CMOS | 28 nm bulk CMOS | | |

$^{\#}$ does not mention circuits included
$^{\dagger}$ single tone excluding residual LO leakage
* including LO/Clock driver; only RF-Low active
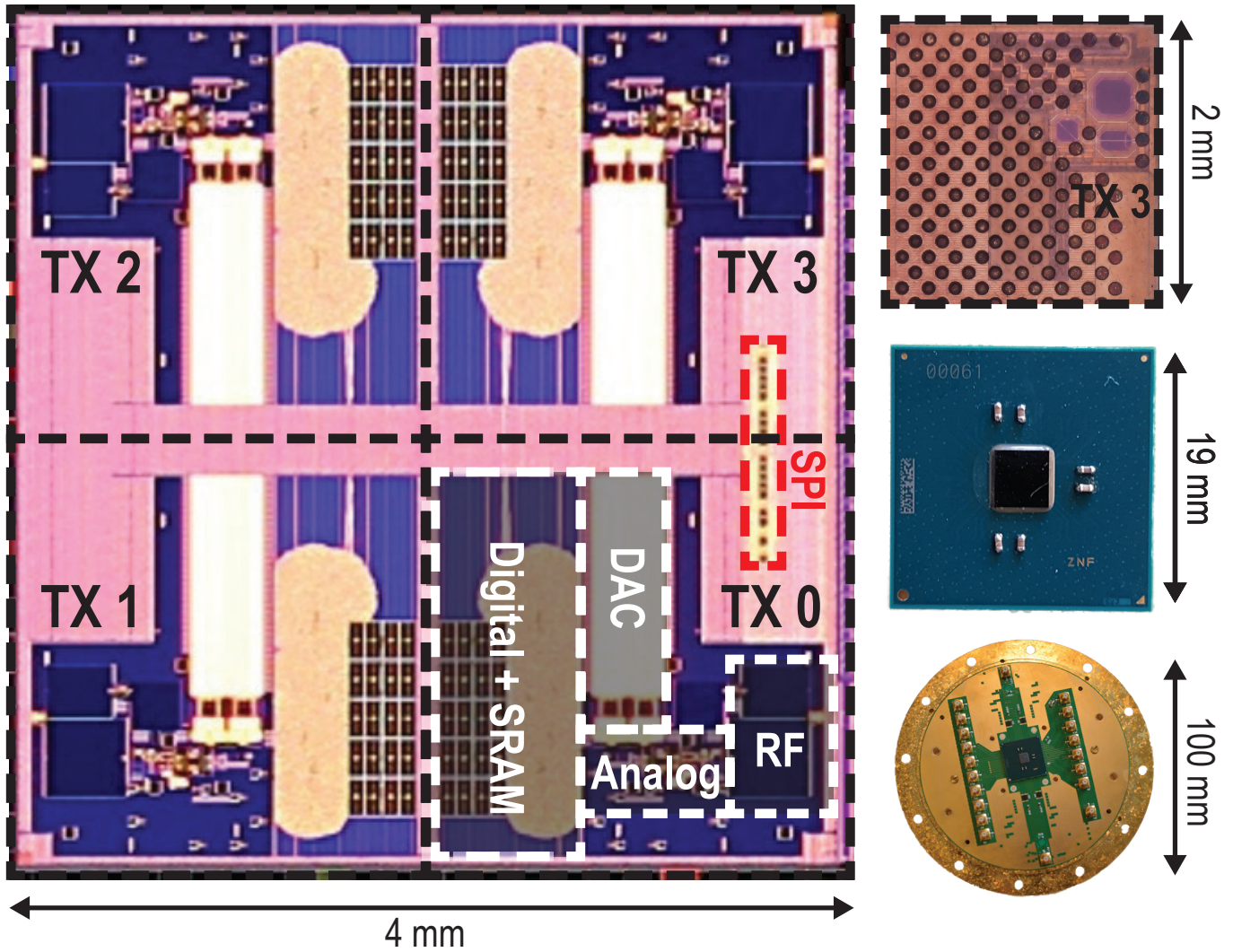$^{\ddagger}$ can be reduced with clock gating

**Fig. 6: Comparison table.**

Fig. 7: Die micrograph (without metal layers) with cut-out of a single transmitter showing I/O bumps and RF transformers, chip package and PCB with enclosure.
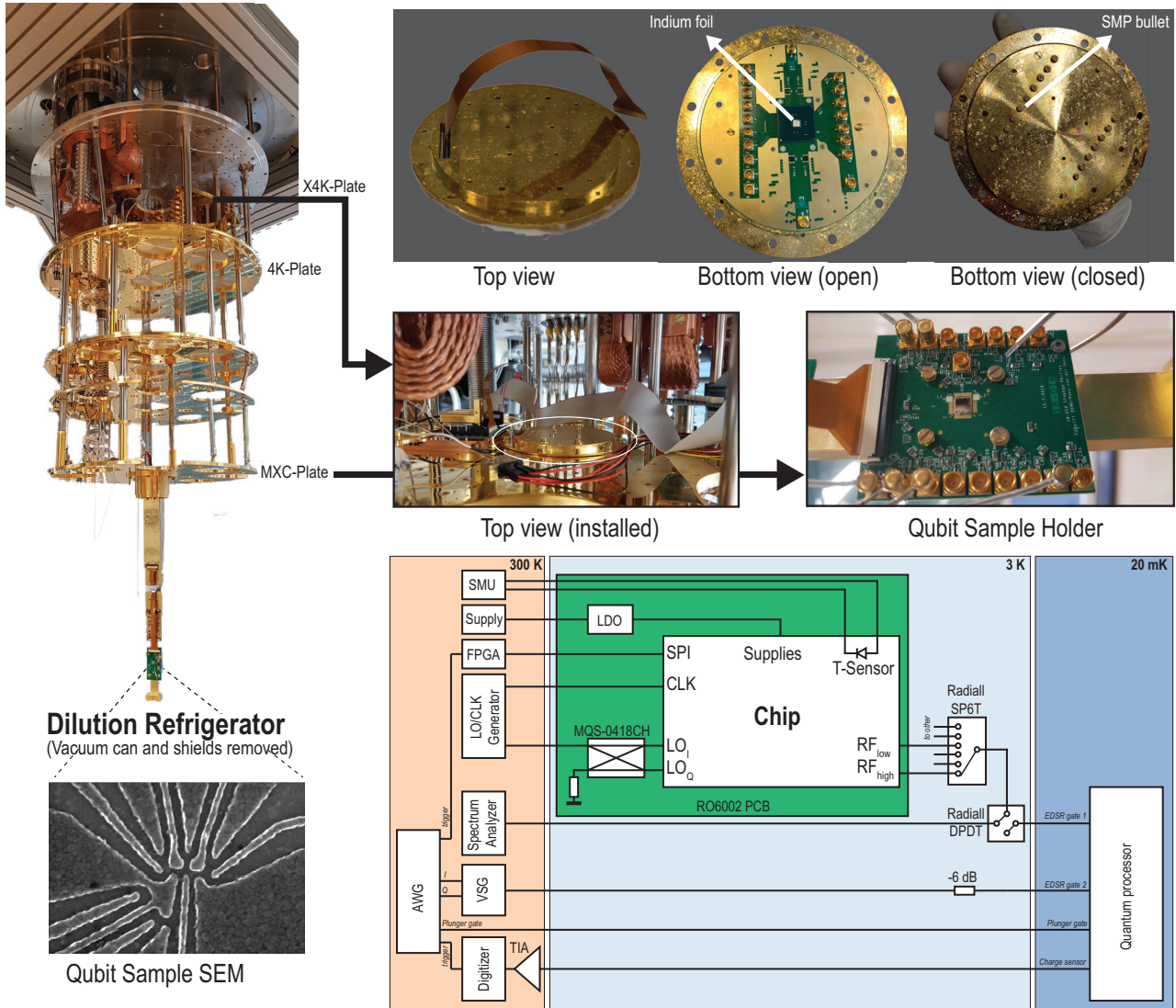
**Fig. S1:** Top to bottom, left to right: dilution refrigerator, qubit sample SEM, PCB enclosure (open & closed), chip and qubit mounting in the fridge and measurement setup block diagram.
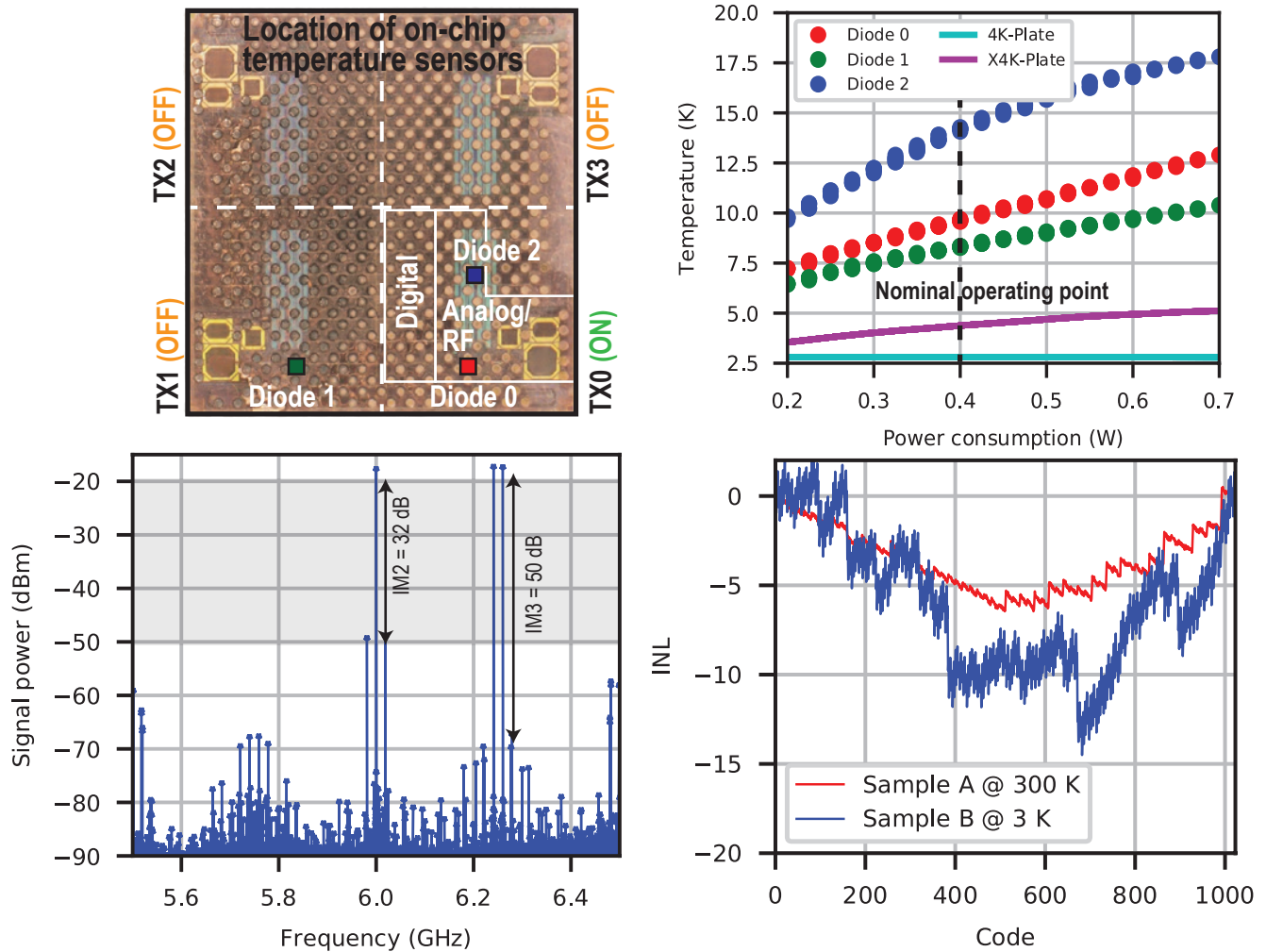
**Fig. S2: Measurement of on-chip and dilution refrigerator temperature sensors (chip is mounted on extra 4K [X4K] plate) by sweeping the power consumption outside the nominal operating point using clock frequency and digital supply voltage, full RF-Low two-tone spectrum at 3 K and DAC INL measurement explaining the observed 2nd order distortion.**
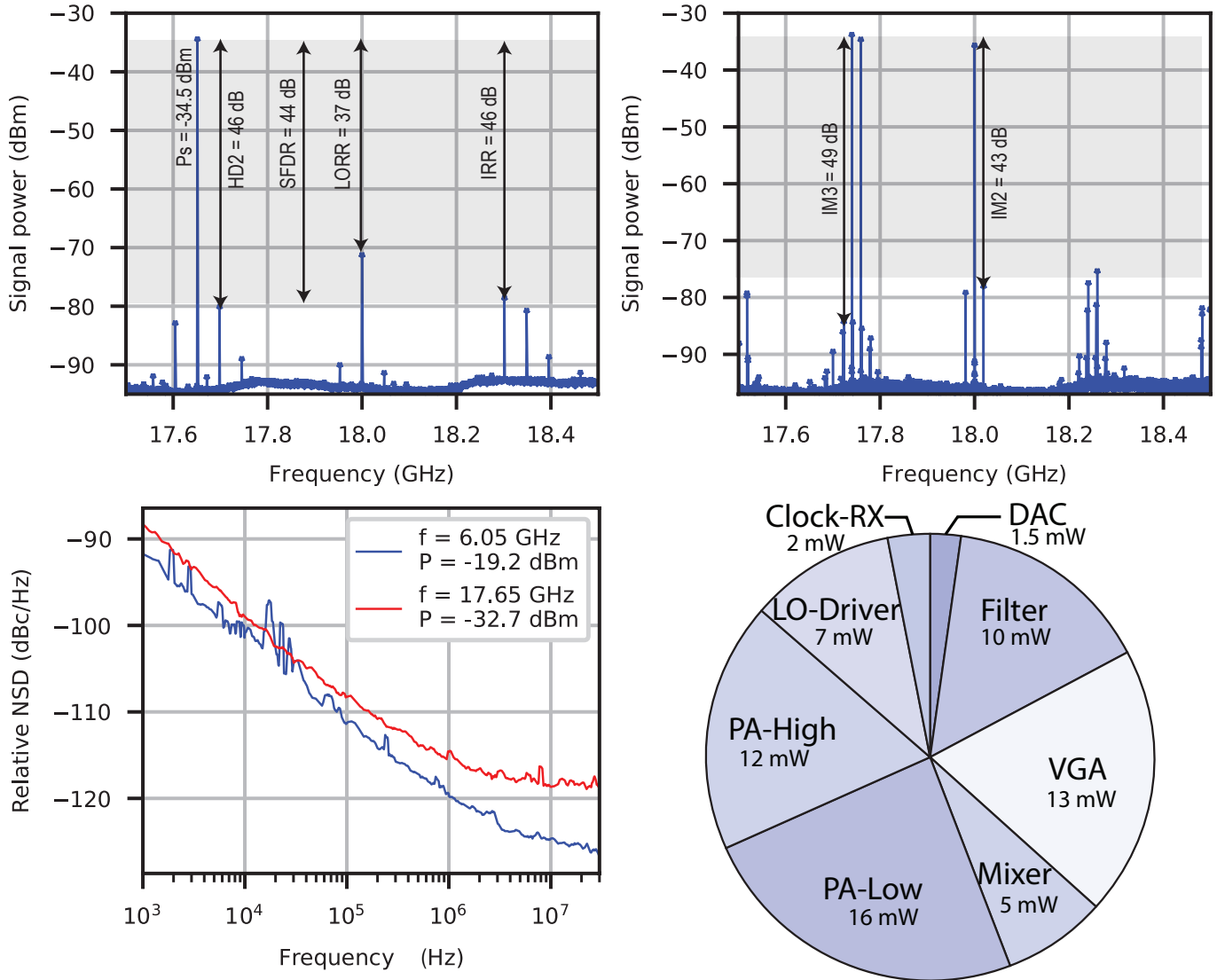
Fig. S3: RF-High output with NCO at 350 MHz, Two-tone RF-High output with NCOs at 241 MHz & 260 MHz, Noise spectral density and power consumption of various circuit blocks, all at 3 K.